Postprint of: Dąbrowski P.: Thermohydraulic maldistribution reduction in mini heat exchangers APPLIED THERMAL ENGINEERING Vol. 173 (2020), pp.1-17 DOI: 10.1016/j.applthermaleng.2020.115271

Paweł DĄBROWSKI*
*pawel.dabrowski@pg.edu.pl; Faculty of Mechanical Engineering, Department of Energy and Industrial Apparatus, Gdańsk University of Technology, Gabriela Narutowicza 11/12, 80-233 Gdańsk, Poland

THERMOHYDRAULIC MALDISTRIBUTION REDUCTION IN MINI HEAT EXCHANGERS

Abstract*:* A detailed numerical investigation has been carried out to analyze the flow maldistribution in 50 parallel 1 mm x 1 mm rectangular minichannels and 1 mm depth minigap section with rectangular, trapezoidal, triangular or concave manifolds in Z-type flow configuration. The working medium was ethanol and the mass flow rate was 5×10^{-4} kg/s. Both sections were heated from the bottom side. Heat flux of 10 000 W/m^2 and 5 000 W/m^2 was applied to the minichannel and minigap section respectively. The method of the flow maldistribution mitigation in the diabatic flow has been checked. Thanks to introducing a threshold, the maldistribution coefficient can be reduced about twice in the minigap section or three times in the minichannel section with the 0.5 mm threshold as compared to the conventional arrangement. The velocity profile and temperature profile over the heat exchanger's surface have been analyzed. Reduction of the maldistribution results in lower maximum temperature over the surface. The distribution is more uniform in the minichannel section than in the minigap section. This is due to a two-dimensional flow over a minigap. Hence, a two-dimensional approach to define maldistribution coefficients in minigap sections, which has not been distinguished in literature yet was used.

Keywords: minichannel; minigap; manifold shape; threshold; numerical study; maldistribution mitigation

1. Introduction

All industries are endeavoring to miniaturize products with simultaneous performance improvement. Miniaturization leads to a reduction in the heat transfer surface of the products and an improvement in performance results in increased heat generation. This causes a significant increase in heat flux density, which should be dispersed from the surface of the devices. As can be seen from Nusselt number definition, smaller the hydraulic diameter, higher the Nusselt number so higher the heat transfer coefficient. That is the reason for the big interest of minichannels or minigaps in cooling or heating.

The minichannel heat exchanger was used for the first time by Tuckerman and Pease [1] to lower the temperature of Very-Large-Scale Integrated Circuits. This was the beginning of miniscale cooling. Since then, the utilization of heat exchangers with minigeometries has become very popular. Research on them began to be carried out around the world, and the industries in which they are used are still increasing. There are among others: space industry [2], solar industry [3], power industry [4], automotive industry [5], avionics industry [6], cryogenic industry [7,8], refrigeration industry [9], chemical and biological industry [10,11].

Mini heat exchangers (utilizing minichannels or minigaps) are characterized by a high heat transfer coefficient and good compactness. However, a small diameter of the channel causes a low mass flow rate of fluid that is able to flow through it (to avoid high pressure drops) and slight heat flux that can be transferred through the surface as a result. That is a reason for the application of many parallel minichannels with common inlet and outlet manifold. But this kind of construction causes a non-uniform or irregular flow of fluid in individual channels, so-called flow maldistribution [12]. It happens that during heat exchangers designing a uniform flow over the entire surface is assumed [13]. This assumption is false and neglecting the maldistribution phenomena can result in non-uniform temperature distribution along the heat exchanger, presence of hot-spots, channels blockage, increase in pressure drop and efficiency reduction [14–19].

The maldistribution phenomenon is not examined well enough and there are disagreements in reports about influencing factors, models for prediction and approaches for mitigation. Moreover, there are a lot of works that are dealing with a flow maldistribution in parallel minichannels

[5,6,9,12,14,20–23] but few that mentioned about flow non-uniformity and non-uniform temperature profile in minigaps [24–26].

Although the flow maldistribution is caused by the hydrodynamics of the flow, the study of flow distribution only in adiabatic conditions poses very little importance [27]. It is the temperature distribution in the presence of heat exchange processes that is the key to the design of cooling or heating systems. Hence, more and more researchers are using infrared techniques or numerical simulations to obtain the temperature profile in minichannels or minigaps [28–30]. Many of them note that temperature distribution is not uniform, which hinders the analysis of other key phenomena, such as heat transfer coefficient quantification. There is a need to develop new solutions to mitigate the flow maldistribution so that neglecting this phenomenon would be justified in researches aimed at other thermohydraulic parameters.

Many authors tried to found this solution. Most of them are focused on geometrical modifications of channels or manifolds. An analytical model aimed at optimizing the shape of the collectors in terms of flow distribution while keeping the manifolds sizes minimum was proposed by Saeed and Kim [31]. The mathematical model was written in the Matlab environment and then numerically verified using the ANSYS-CFX code. The authors simulated the work of heat exchangers with various amounts of minichannels (from 22 to 92). The water was assumed as a working fluid and a volumetric flow rate of 8.3 to 25 cm^3/s was set at the inlet. Studies have shown that as the flow rate increases, the flow maldistribution coefficient increases. The shape of collectors optimization allowed to improve the distribution by up to 74%, while reducing the pressure drop by 71%. The numerical simulation in ANSYS Fluent 16.0 code was done by Tang et al. [32]. The authors examined the Self-Similarity Heat Sink (SSHS) and proved that a significant flow maldistribution exists inside SSHS. The authors conducted numerical simulations for five different mass flow rates and a constant heat flux density of 1.5 MW/m^2. To improve the fluid distribution, modifications to SSHS structure (inlet manifold channel and the inlet plenum) were done. The tapered contracting structure was proposed to mitigate the maldistribution phenomenon. A more uniform flow resulted in a 24 K decrease in the maximum temperature of the heat exchanger. The numerical study on mitigation of the flow maldistribution in parallel microchannels was done by Kumar et al. [33]. The authors proposed a new idea that is based on varying the width of parallel channels (VWMCHS). Increasing the width of those channels in which the velocity is low and decreasing the width in those channels in which the velocity is high results in a more uniform mass flow rate in channels. It is noticed that a new design mitigates the maldistribution coefficient of the conventional design by 93.7%. Hydraulic uniformity also brings thermal uniformity. The same authors have studied their approach more [34] and carried out a new solution based on variable height microchannels (VHMCHS). The average surface temperature on the heat exchanger was reduced by 3.3 K for the VHMCHS compared to VWMCHS. Also, the heat transfer coefficient has been improved by 3.8% (VWMCHS) and 5.1% (VHMCHS) compared to the classic design with a fixed width and height of channels. Both approaches effectively improve flow distribution in parallel channels. Anbumeenakshi and Thansekhar [35] performed the experimental investigation of manifold shape and configuration on flow maldistribution. This experiment showed that inline flow configuration results in worse fluid distribution than vertical flow inlet configuration. Also, the mass flow rate influences the distribution of fluid. The authors concluded that the best distribution is obtained when fluid flows into a rectangular inlet manifold perpendicular to the length of the manifold at high flow rates.

As can be seen from the above considerations, a lot of papers [31,32,35] focus on the modification of manifolds to improve the distribution of the fluid. In research on the maldistribution phenomenon, some authors focus only on the hydrodynamics of flow and choose adiabatic conditions in their considerations [14,20,23,35] and others take into account heat transfer [31–34]. The current study shows a method of flow maldistribution reduction that was numerically investigated before in adiabatic conditions [36]. This study tested the solution in the scope of the heat flow rate in minichannels and minigaps. There are few investigations concentrated on non-uniformity in minigaps or which compare minigaps with minichannels [24,26]. It seems like some researchers are using the term of minichannel and minigap interchangeably. However, the flow in minigap is different than the flow in minichannel. The presented study showed that flow in minigap is two-dimensional. The velocity vector in a direction

perpendicular to the main flow direction is significant and cannot be neglected. Hence, the velocity profile is complex and thus temperature profile is much more uninform compared to minichannel sections. Therefore, there is a need for in-depth study to take a closer look at fluid flow in minigap sections and to compare minigaps with minichannels, showing differences between them. In the present work, a detailed numerical investigation was carried out to examine the effect of threshold on flow distribution through the minigap and minichannel sections taking into account the maldistribution effects in the form of a temperature profile. The presented approach is new in terms of diabatic flows. It can be simply used in practice to avoid maldistribution in researches where the possibility of maldistribution neglect would be useful or in commercial heat exchangers to reduce the hotspots. The two-dimensional maldistribution calculations in the minigap section have not been found in literature yet.

2. CFD model details

Before starting the numerical simulation, the mini heat exchangers with 4 different shapes of inlet and outlet manifolds have been designed. Three-dimensional models were created with the Autodesk Inventor software. Then, they were exported to the ANSYS SpaceClaim software and the fluid domains were prepared. The working medium was assumed as ethanol. The fluid flows in the opposite direction to the Z and X axes. The ethanol was heated up from the bottom of the section (in the opposite direction to the Y axis). The constant heat flow rate was applied for the minigap and minichannel sections. The material of the heat exchanger was assumed as copper, the thickness of wall transporting heat to the ethanol was equal to 9 mm. The inlet and outlet manifolds were not heated up. Whole heat was transported to the minigap or minichannels.

2.1. Physical model

Two kinds of a section in Z-type flow configuration, namely minigap and minichannel section have been taken into account. The physical models of mini sections have been shown in Fig. 1 and all their specific dimensions were summarized in Table 1. In the numerical simulation, sections were connected with inlet and outlet manifolds with various shapes, namely rectangular, trapezoidal, triangular and concave. Mentioned manifolds and their dimensions have been shown in Fig. 2. The flow maldistribution mitigation approach, which was previously tested [36] in adiabatic conditions has been implemented in thermohydraulic calculations. This approach consists in introducing threshold t at the entrance of the minigeometry section. The threshold has been employed by making a manifolds' depth d bigger than the section's depth.

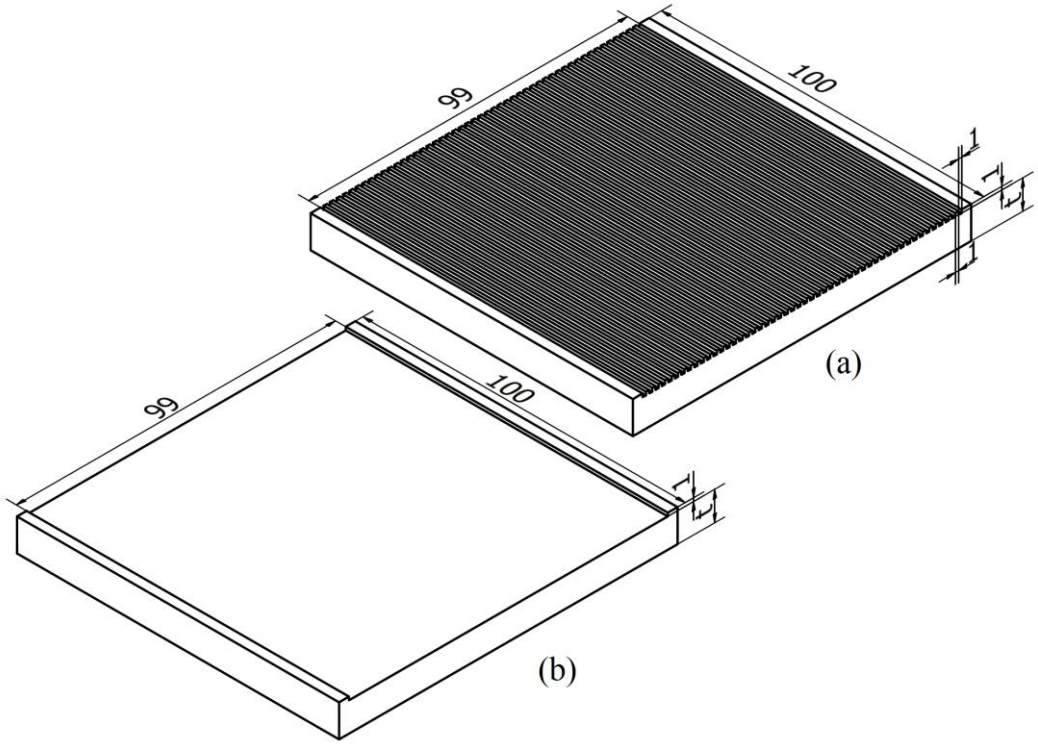

Fig. 1 Physical model of sections used in the numerical simulation (a) minichannel section (b) minigap section

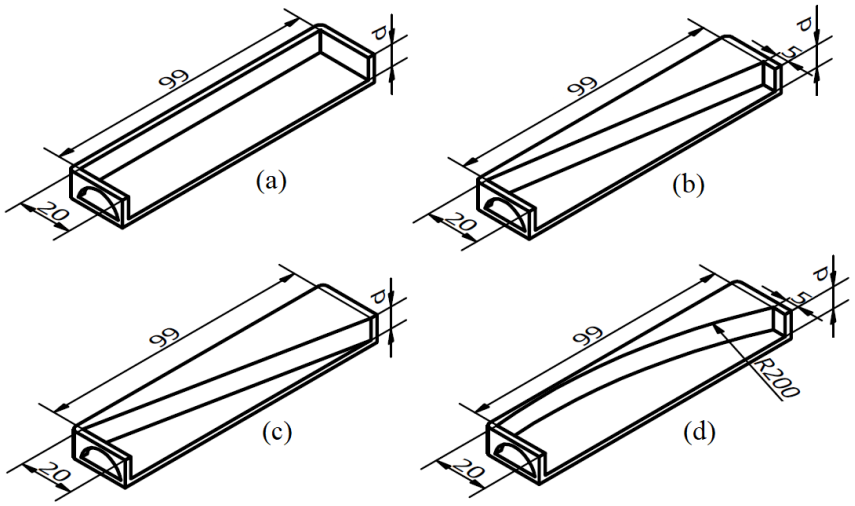

Fig. 2 Physical model of manifolds used in the numerical simulation (a) rectangular (b) trapezoidal (c) triangular and (d) concave

Table 1 Geometrical parameters of the sections

Section			
Minichannel		**Minigap**	
Parameter	**Value**	**Parameter**	**Value**
Depth	1 mm	Depth	1 mm
Width	1 mm	Width	99 mm
Hydraulic diameter	1 mm	Hydraulic diameter	1.98 mm
Fin spacing	1 mm		
Number of channels	50		

The examples of the whole fluid domains (section and inlet/outlet manifolds) that were taken into account have been shown in Fig. 3 and Fig. 4. Fig. 3 shows the minichannel section with rectangular

manifolds and Fig. 4 shows the minigap section with trapezoidal manifolds but there were 8 minichannel cases, namely minichannel section with rectangular, trapezoidal, triangular or concave manifolds without thresholds and with 0.5 mm thresholds as well. There were also 8 minigap cases combined with the same manifolds as previously (4 shapes with and without threshold).

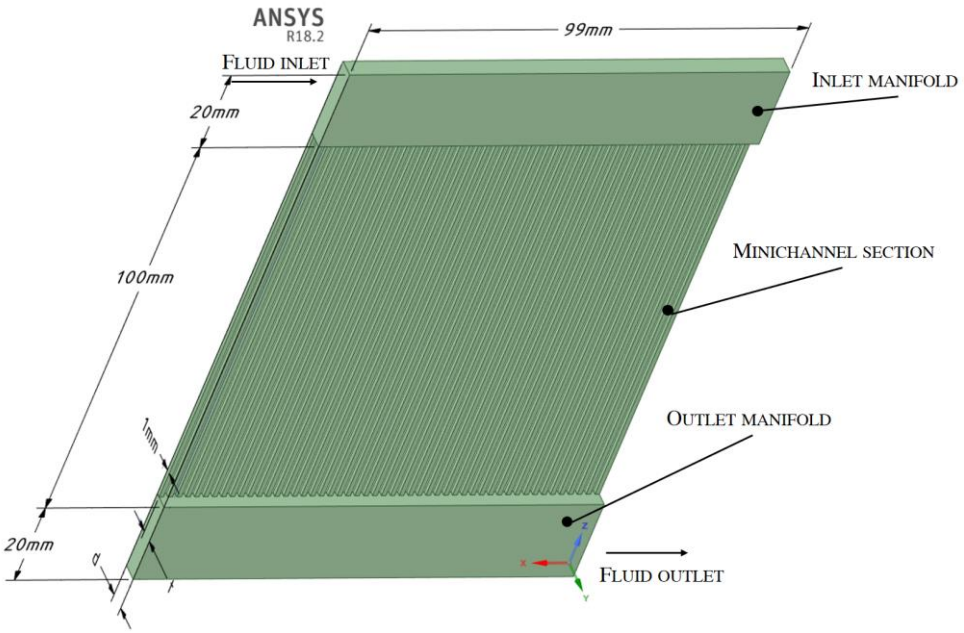

Fig. 3 The fluid domain of minichannel section with rectangular manifolds

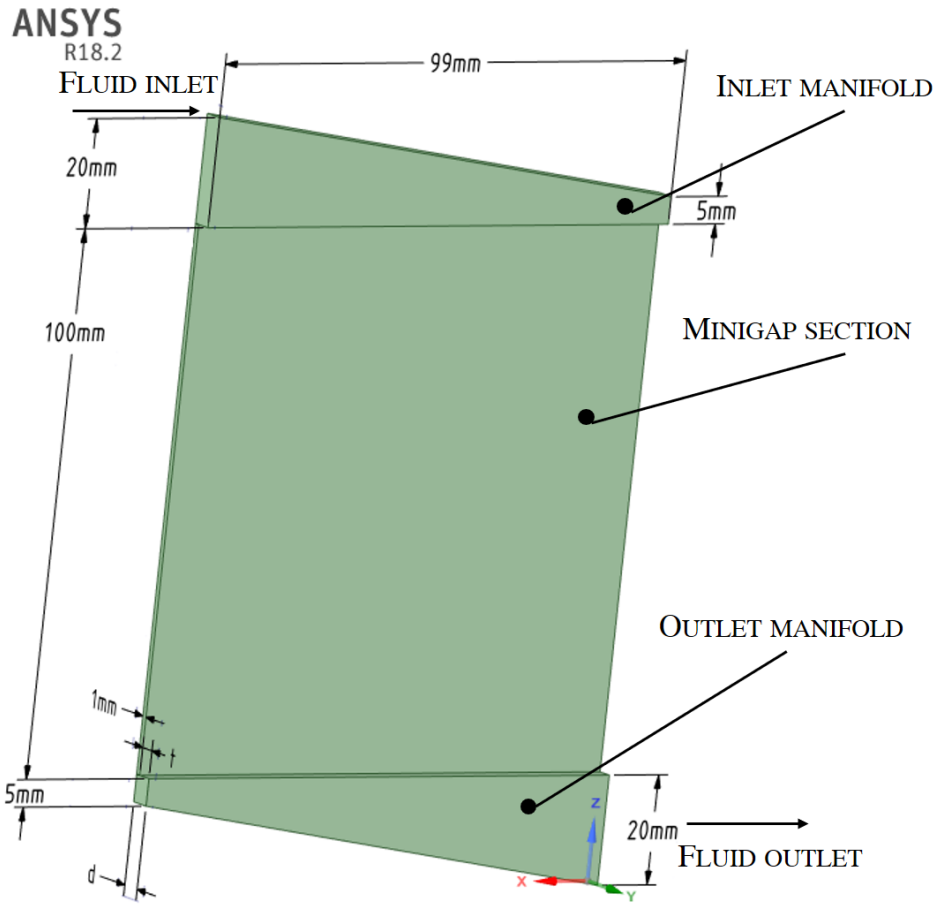

Fig. 4 The fluid domain of minigap section with trapezoidal manifolds

2.2. Governing equations and boundary conditions

To investigate the effect of the threshold at the entrance of the minigeometry section on flow maldistribution and to compare the temperature fields on minichannel and minigap heat exchangers the following assumptions were taken:

- Properties of fluid were independent of temperature and pressure.
- Fluid flow was a single-phase, steady-state, incompressible and three-dimensional.

The continuity, momentum and energy equations (Eq. (1), Eq. (2) and Eq. (3)) were taken into account as governing equations and used in calculations together with the above-mentioned assumptions.

$$\nabla \cdot \vec{V} = 0 \tag{1}$$

$$\rho(\vec{V} \cdot \nabla \vec{V}) = -\nabla p + \mu \nabla^2 V \tag{2}$$

$$\rho C_p(\vec{V} \cdot \nabla T) = k_f \nabla^2 T \tag{3}$$

The gravity acceleration g=9.81 m/s^2 is consistent with the direction of the Y-axis.

In ANSYS FLUENT 18.2 the conservation equations of mass, momentum and energy are solved using finite volume method (FVM). Momentum and energy equations are discretized by the second-order upwind scheme. Various turbulence models have been considered, namely SST k-omega; SST k-omega Low-Re; Laminar and Spalart Allmaras. There are no significant differences in the velocity field, pressure drop or temperature distribution in channels between models (Table 2). In this case model SST

k-omega has been chosen as a turbulence model. As known, this model gives good results near a wall, which is desirable in small channels and good results in bigger volume, which is desirable in bigger manifolds (with threshold) [37,38]. A segregated implicit solver with Coupled pressure correction algorithm has been chosen to compute the velocity field in the whole heat exchanger (inlet/outlet manifolds and mini section).

Ethanol was chosen as a working fluid for all the considered cases. The inlet parameters for ethanol are $\rho = 754.3$ kg/m^3, $\mu = 5.86\times10^{-4}$ Pa s, C_p=2.99 kJ/kg K, k_f=0.16 W/m K and T=333.15 K. The heat was applied at the bottom wall of a section (gap or channels) with a constant value of heat flux $\dot{Q}$ of 10 000 W/m^2 for minichannels and of 5 000 W/m^2 for minigap. The heat flux for minigap was 2 times smaller, because of 2 times bigger area in minigap than in the minichannel section. This resulted in the same heat flow rate of about 50 W applied to the sections' surface. The constant mass flow rate at the inlet to the heat exchanger was equal to 5×10^{-4} kg/s. The pressure-outlet boundary condition was assumed at the outlet of the heat exchanger. The mean velocity V_m in a single minichannel and minigap was 0.01 m/s and mean Reynolds number R_m was 17.1. When the residual values become less than 10^{-6} for the continuity, x-velocity, y-velocity, and z-velocity and 10^{-9} for the energy the solutions are considered to be converged.

Table 2 Pressure drop and the average temperature in channels for minichannel section with rectangular manifolds with a threshold for different turbulence model

	Pressure drop [Pa]	**T_{avg} in channels [K]**
SST k-omega	41.51	351.70
SST k-omega Low-Re	41.52	351.70
Laminar	41.51	351.70
Spallart Allmaras	41.52	351.70

3. Model validation

To validate the model the normalized velocity V_n was used. The normalized velocity is a ratio of the actual velocity at the considered point of the section (e.g. in i-th channel) to the mean velocity (velocity that would occur in every channel if the flow will be fully uniform). The first channel (i=1) is the nearest to the fluid inlet and the last channel (i=50) is the nearest to the fluid outlet. The mathematical expression of normalized velocity has been shown in Eq. (4).

$$V_{n,i} = V_i / V_m \tag{4}$$

Fluid domain was discretized using ANSYS Fluent with tetrahedral control volumes in manifolds and hexahedral control volumes in channels or gap. The mesh independence study was carried out to ensure the accuracy of numerical results. There were three different mesh types tested: Coarse (7.0×10^5 elements), Medium (2.2×10^6 elements) and Fine (3.8×10^6 elements). The results of the minichannel section with rectangular manifolds with a threshold grid independence study were shown in Fig. 5. Results showed that the absolute percentage deviation between Medium and Fine mesh type is less than 1% for pressure drop and the average temperature in channels as well. Moreover, the normalized velocity distribution in channels was checked for different mesh types. It was shown in Fig. 6. The Medium and Fine mesh results in almost identical normalized velocity distribution in channels, which suggest the independence of mesh on results. The Medium mesh has been chosen for further calculations.

Computational mesh consisted of about 1.2×10^6 and about 2.2×10^6 elements for minichannel section with conventional manifolds and with novel manifolds respectively. Computational mesh consisted of about 2.5×10^6 elements for minigap sections regardless of manifold type.

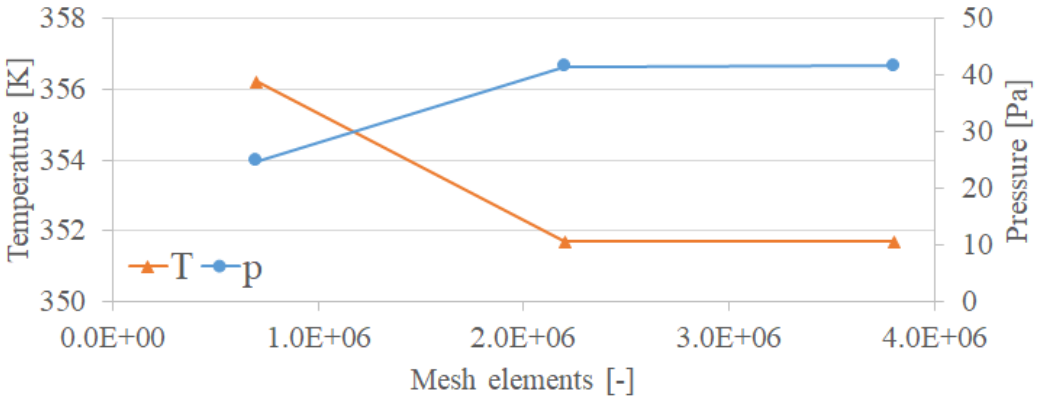

Fig. 5 The results of grid independence study. T - the average temperature in channels, p – pressure drop in channels. CFD simulation made for the minichannel section with rectangular manifolds with a threshold.

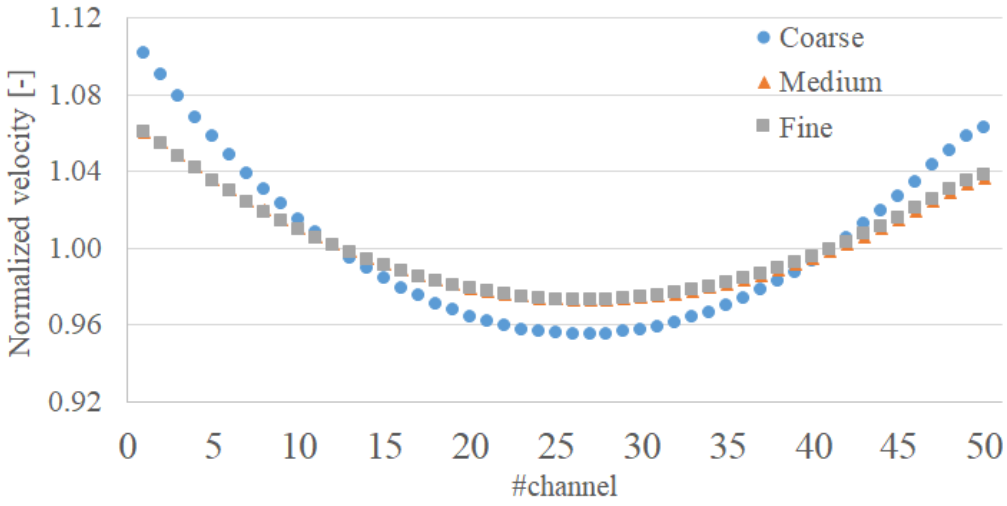

Fig. 6 The comparison of normalized velocity in the minichannel section with rectangular manifolds with a threshold for different mesh types.

Current numerical model is verified by comparing values of simulated local Nusselt number in minichannel section with conventional rectangular manifold with theoretically developed correlation of Lee and Garimella [39]. The Nusselt number from silumation was calculated using Eq. (5). Results of comparative analysis of local Nusselt number are shown in Fig. 7. Maximum deviation in local Nusselt number are found to be 14.3%. A good agreement between current model and theoretical correlation ensures the accuracy and reliability of current numerical analysis.

$$Nu = \frac{qD_h}{k_f (T_w - T_f)} \tag{5}$$

To validate a model that was utilized during the calculations, it has been made an experiment with a minichannel heat exchanger with conventional trapezoidal manifolds (without threshold). The infrared camera was used to determine the velocities in channels and then the maldistribution. The method from [18] was used to quantify fluid distribution over the heat exchanger. Fig. 8 shows the normalized velocity from the experiment and from the simulation. Thanks to velocity distribution in channels, the maldistribution coefficient could be calculated from Eq. (6). Its distribution has been shown in Fig. 9.

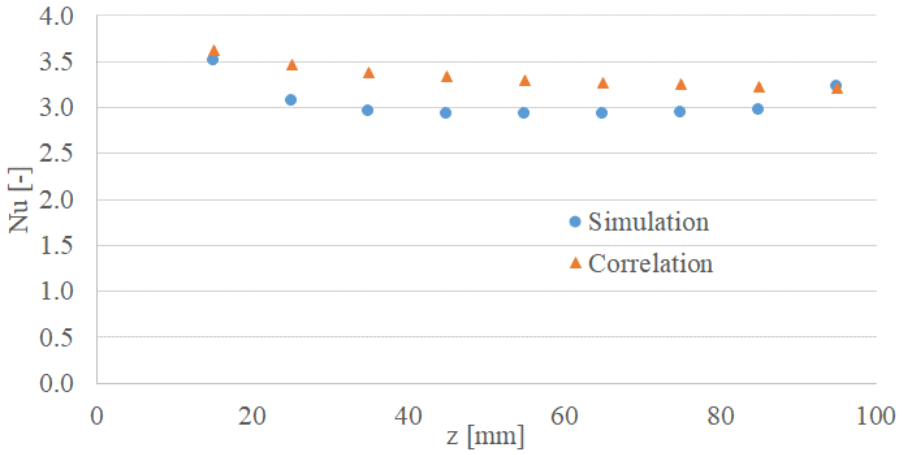

Fig. 7 Comparison of local Nusselt number for minichannel section with rectangular manifold without threshold. Simulation results and correlation from Lee and Garimella [39]

$$\Phi_i = \frac{|V_i - V_m|}{V_m} \times 100\% \tag{6}$$

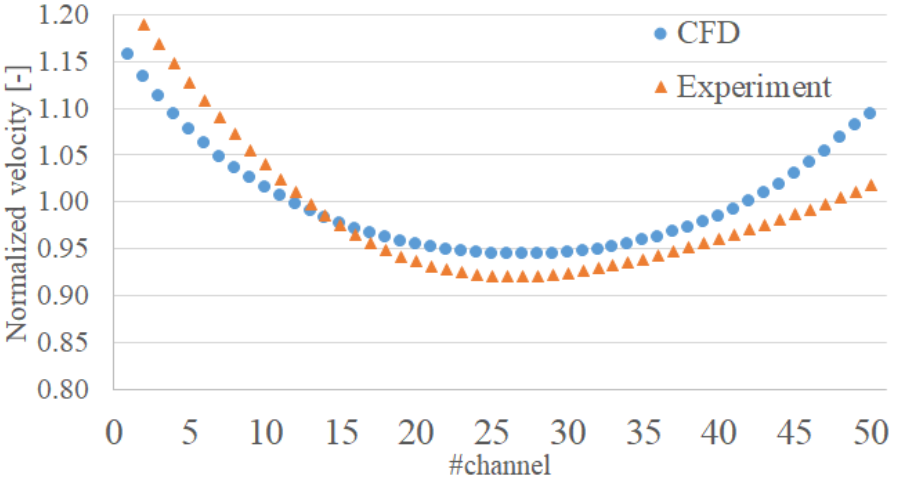

Fig. 8 The comparison of normalized velocity in the minichannel section with trapezoidal manifolds without a threshold for experiment and CFD simulation.

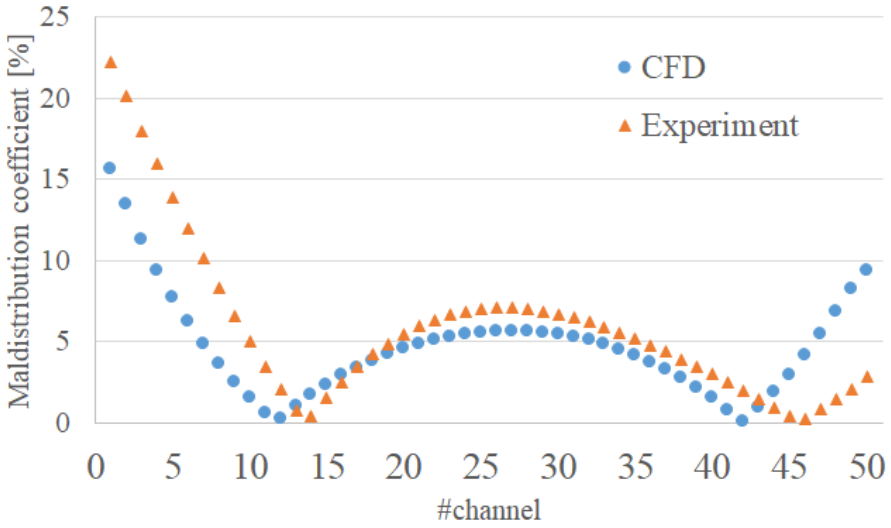

Fig. 9 The comparison of the maldistribution coefficient in the minichannel section with trapezoidal manifolds without a threshold for experiment and CFD simulation.

4. Results and discussion

The author numerically analyzed 16 cases in terms of flow maldistribution. There were 8 cases for minichannel section with rectangular, trapezoidal, triangular or concave manifolds (with and without threshold) and 8 cases for minigap section with rectangular, trapezoidal, triangular or concave manifolds (with and without threshold). The mass flow rate of 5×10^{-4} kg/s was constant for all cases. For every single case, the flow velocity and temperature profile were obtained. Then, the flow maldistribution coefficient in i-th of 50 channels in the minichannel section was calculated from Eq. (7). In the minigap cases, a two-dimensional approach to calculate the total flow maldistribution coefficient was used. Firstly, ten XY planes (every 10 mm: Z=0 mm, Z=10 mm, Z=20 mm etc.) were chosen along the minigap to show the differences of flow in the Z-axis. Fifty points (in X-axis direction) were distinguished on each XY plane (to make it comparable with 50 channels in minichannel sections) and at those points the calculations of the maldistribution coefficient (Eq. (6)) were carried out.

The overall maldistribution coefficient in every case was calculated as a standard deviation of N=50 previously calculated points (Eq. (7)). Moreover, for minigap cases, the overall maldistribution coefficients for each of ten XY planes have been averaged using the geometric mean to obtain one value for every minigap case. The geometric mean was chosen because of the geometric size distribution for subsequent XY planes.

$$\Phi_o = \frac{\sum_{i=1}^{N}\Phi_i}{\sqrt{N}} = \frac{1}{\sqrt{N}}\sum_{i=1}^{N}\frac{|V_i - V_m|}{V_m}\times 100\% \tag{7}$$

Fig. 10 shows that introducing threshold before the entrance of the minichannel section results in reducing the maldistribution coefficient. There are no significant differences in the maldistribution coefficient for various manifolds after introducing threshold except the triangular manifold. The maldistribution coefficient for conventional and novel cases is 46% and 15%, 33% and 11%, 23% and 20%, 34% and 11% for rectangular, trapezoidal, triangular and concave manifolds respectively. The reduction for all manifold types except the triangular one is about 3 times.

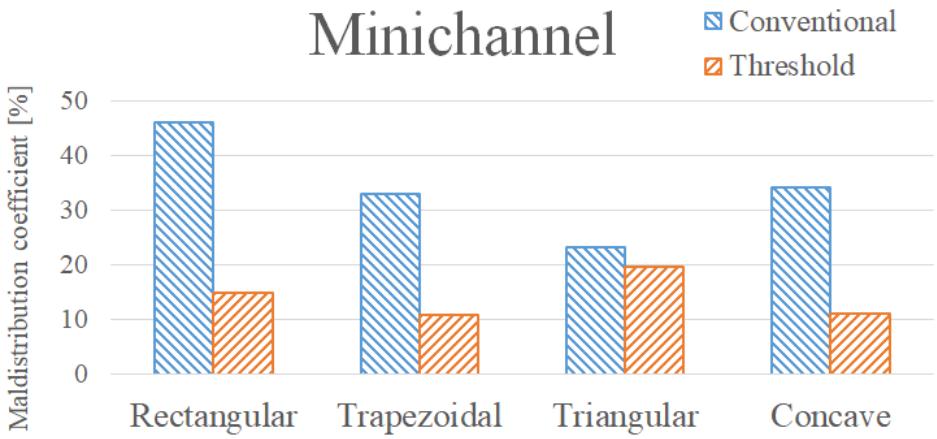

Fig. 10 The maldistribution coefficient in a minichannel section for various manifolds. The comparison of the conventional case (without threshold) and novel case (with threshold).

Additionally to the standard cases mentioned earlier, the channels' length influence studies were carried out for rectangular manifolds with and without threshold. It was done just to find and describe the general trend of channels' length influence on flow maldistribution coefficient and not the specific maldistribution coefficients for every single manifold geometry and various channels' lengths. There were 3 lengths that were tested: L=100 mm, L=50 mm and L=10 mm. Fig. 11 shows the results of the mentioned studies. It can be seen that flow becomes more uniform when the channels' length decreases. It corresponds with conclusions from other researchers [40,41]. Regardless of the channels' length, the proposed method of reducing the flow maldistribution is effective. The flow maldistribution coefficient can be reduced 3.1, 3.0 and 2.3 times after threshold introduction for L=100 mm, L=50 mm and L=10 mm respectively. The decreasing length of channels results in decreasing pressure drop in them. The averaged pressure drops in channels of L=100 mm, L=50 mm and L=10 mm are 41.5 Pa, 20.6 Pa and 4.0 Pa respectively. Hence, the ratio of pressure drop in channels to pressure drop in manifolds is increasing with channels' length. This is favorable to flow uniformity [42].

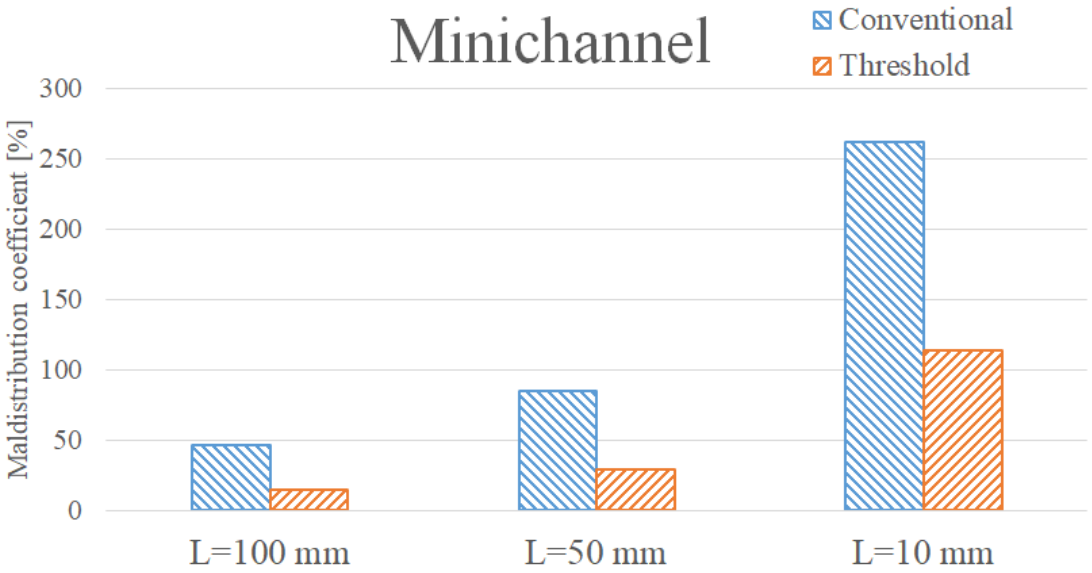

Fig. 11 The maldistribution coefficient in a minichannel section with rectangular manifolds for various channels' lengths L. The comparison of the conventional case (without threshold) and novel case (with threshold).

Fig. 12 shows analogous data as in Fig. 10 but for the minigap section. First of all, it should be noticed that the distribution of fluid in the minigap section is much worse than in the minichannel section. It happens due to two-dimensional flow over a minigap in comparison to one-dimensional flow

in a channel. According to the flow continuity equation, the amount of fluid that enters the channel must be the same as the amount that leaves it. So the mass flow rate of fluid in the Z-direction is constant in separate channels (same at the inlet and outlet of the channel). This situation does not happen in the case of the minigap section. The mass flow rate of fluid in the exact point over the width at the inlet of the section differs from the point at the same X-coordinate at the outlet of the section. The fluid can flow on the diagonal of the heat exchanger. That is a reason why the minigap section suffers more from the non-uniform distribution of fluid. Nevertheless, the proposed solution reduces the maldistribution coefficient in minigap even 2 times. The maldistribution coefficient for conventional and novel cases is 214% and 118%, 242% and 146%, 254% and 164%, 223% and 127% for rectangular, trapezoidal, triangular and concave manifolds respectively.

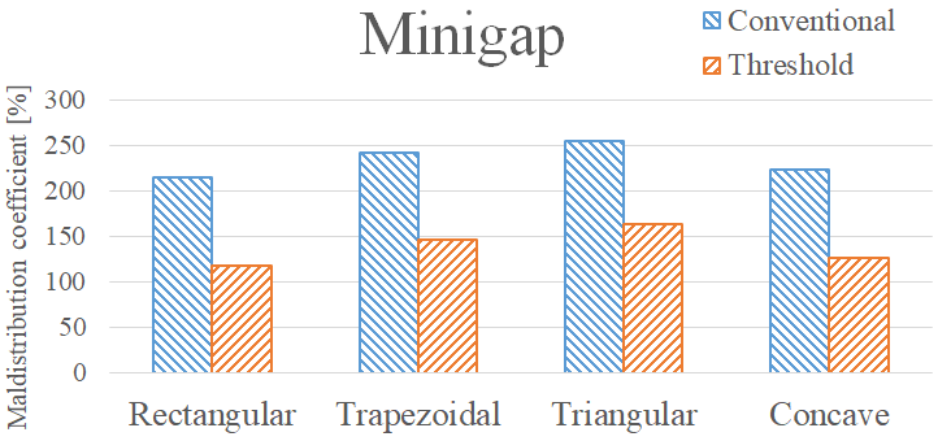

Fig. 12 The maldistribution coefficient in a minigap section for various manifolds. The comparison of the conventional case (without threshold) and novel case (with threshold).

The velocity distribution over the heat exchanger surface depends strongly on the inlet and outlet manifold's shape. The flow distribution in the XZ surface at the center of the channels (0.5 mm above the heating surface) for the minichannel section with various manifolds has been shown in Fig. 13. It is a conventional case without threshold at the entrance of a section. It is seen that the highest velocity, namely 6.2×10^{-2} m/s can be observed in a triangular manifold case. The second highest velocity is 5.5×10^{-2} m/s for a trapezoidal manifold case and 5.3×10^{-2} m/s for both rectangular and concave manifold cases. This high velocity in the inlet triangular manifold is caused by the tiny area near the inlet of the last minichannel (the furthest from the inlet to the heat exchanger). Due to the reduction of the area, the flow velocity is growing to fulfill the continuity equation.

Moreover, it can be observed that the rectangular manifolds have the largest areas where the flow velocity is near 0 m/s. Those places do not take part in the heat exchange. For all other shapes, these surfaces are much smaller or do not appear at all. In almost all cases, except triangular one less fluid flows through the middle channels and more through the side channels. In the triangular manifold case, the flow behaves inversely.

After increasing the depth of the manifolds while the section's depth remains constant (introducing threshold), the velocity profile in the XZ surface at the center of the channels becomes more uniform. The mentioned profile for various manifolds has been shown in Fig. 14. Still, the highest velocity, namely 5.3×10^{-2} m/s can be observed for a triangular manifold case but it is reduced by 0.9×10^{-2} m/s in comparison to the conventional case. More significant maximum velocity reduction, namely 2.3×10^{-2} m/s can be observed for other manifolds.

The proposed maldistribution mitigation approach makes flow more uniform reducing the pressure drop in manifolds. It is similar phenomena as described earlier where the length of channels has been changed. The ratio of pressure drop in channels to pressure drop in manifolds is increasing with manifolds' depth. Moreover, the additional space for fluid in the inlet manifold provides the possibility of stabilization. The fluid fills the entire surface of the collector starting from the bottom, and then the fluid height rises. In this case, the flow front of the working medium flows into all channels at the same time and with a similar flow rate. In a conventional case without a threshold, the channels closest to the

heat exchanger's inlet are fed first with the highest flow rate due to no stabilization in manifold possibility. To mitigate the maldistribution phenomena it should be ensured that fluid fills the entire inlet manifold before it starts to fill the channels. This can be promoted by lowering the hydraulic resistance in the inlet manifold and increasing the hydraulic resistance in channels. Fluid always flows wherever it encounters the least resistance. Only after filling the manifold and increasing the hydraulic resistance in it, the fluid will begin to flow into the channels and it would be done more uniformly.

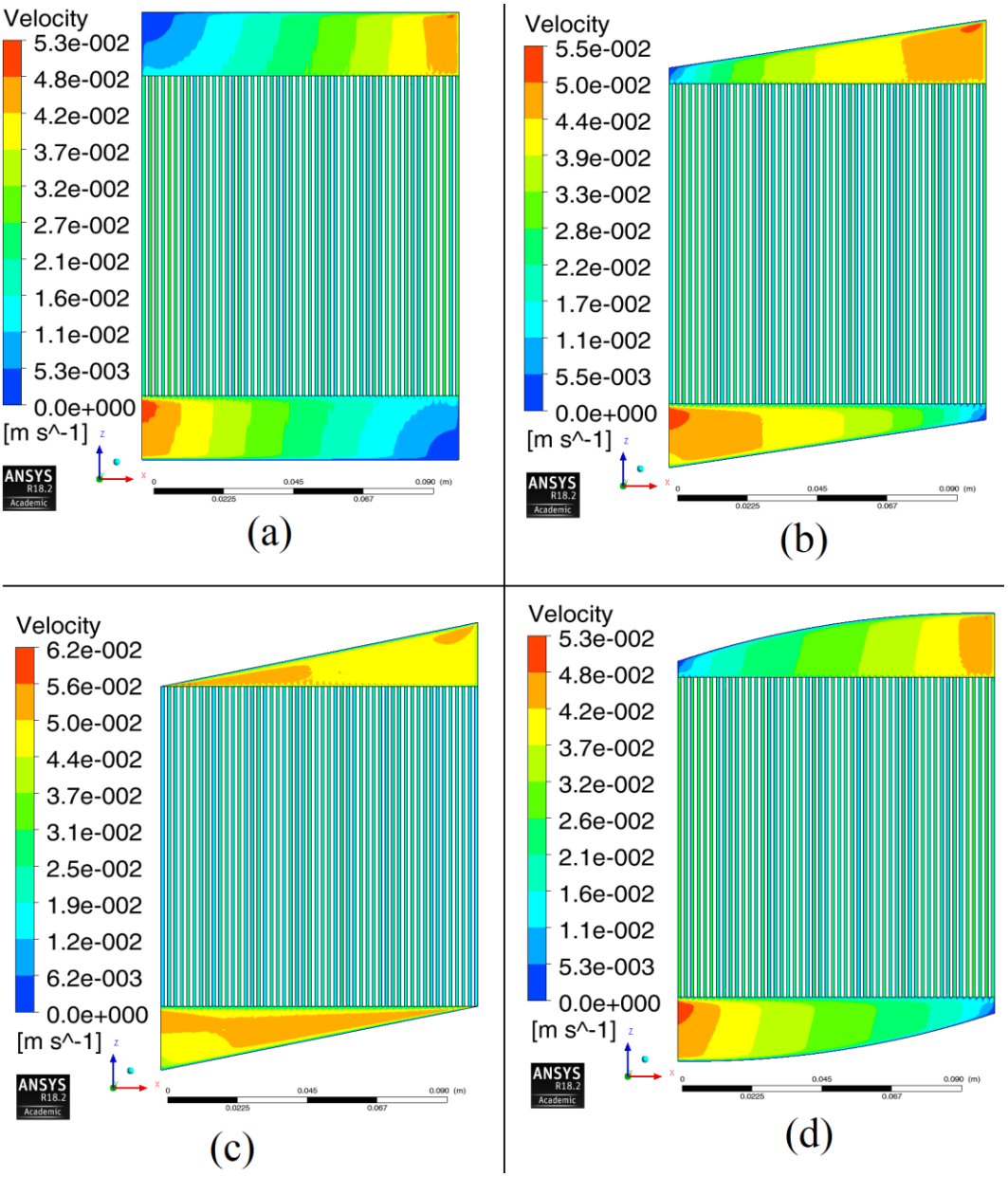

Fig. 13 The velocity distribution over minichannel heat exchanger with various manifolds (conventional case without threshold). Manifolds: (a) rectangular (b) trapezoidal (c) triangular (d) concave.

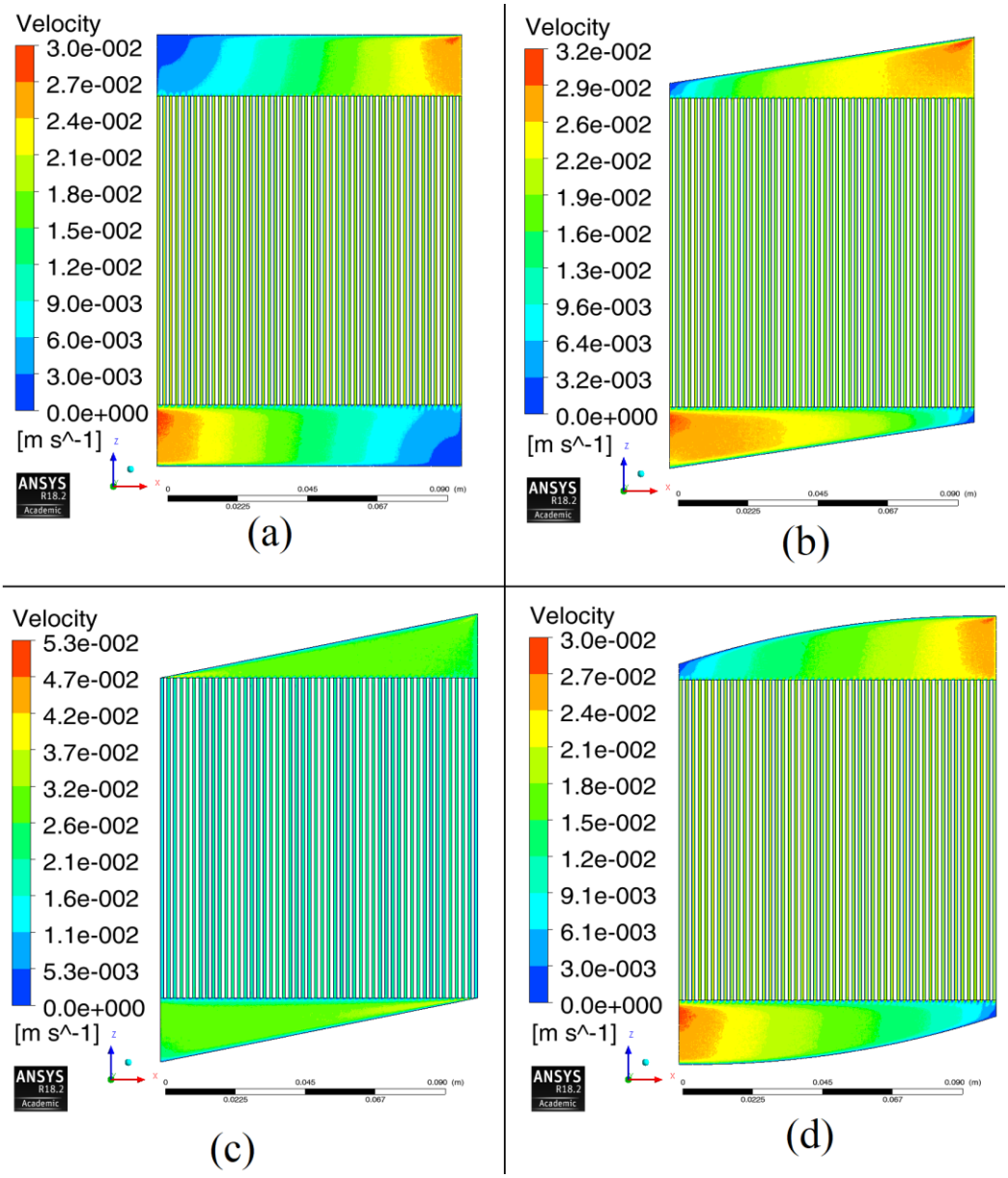

Fig. 14 The velocity distribution over minichannel heat exchanger with various manifolds (novel case with threshold). Manifolds: (a) rectangular (b) trapezoidal (c) triangular (d) concave.

The uniform distribution of fluid over the heat transfer surface is particularly important from the temperature distribution point of view. An extremely unwanted phenomenon is the occurrence of hotspots, which may cause in some cases even burnout of the heat exchanger's wall. The uniform distribution of fluid causes the uniform temperature profile over the heat exchanger's surface. The temperature distribution in the conventional (without threshold) minichannel section with various manifolds has been shown in Fig. 15. The highest temperature is in a triangular manifold case. The points where the temperature is equal to 387 K can be found in those channels, where the mass flow rate is significantly smaller, namely in the first and the last channel. The narrowing of the cross-section near the inlet to the last channel (farthest from the inlet to the heat exchanger) and at the outlet from the first channel (closest to the inlet to the heat exchanger) causes a reduction in a mass flow rate in those channels, and thus a rise in temperature. The isotherms lines in the minichannel section correspond with velocities, the higher the velocity the lower the temperature.

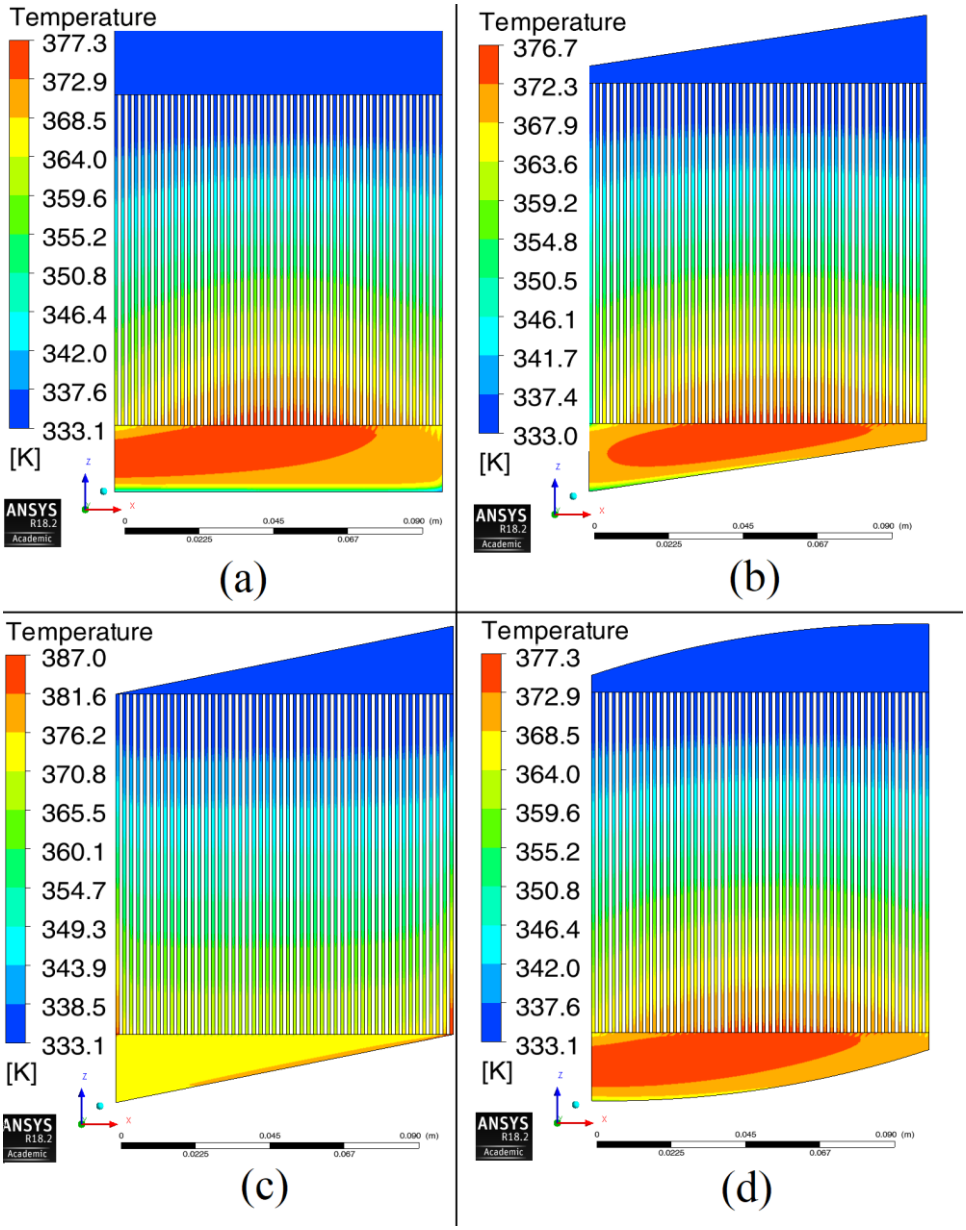

Fig. 15 The temperature distribution over minichannel heat exchanger with various manifolds (conventional case without threshold). Manifolds: (a) rectangular (b) trapezoidal (c) triangular (d) concave.

The temperature distribution in a minichannel section with various manifolds after introducing the threshold has been shown in Fig. 16. The isotherms lines are being more parallel to the width of the minichannel section, which testifies about more uniform flow distribution. The reduction of the highest temperature in each case is 2.9 K, 2.9 K, 1.3 K and 3.3 K for rectangular, trapezoidal, triangular and concave manifold cases respectively. Also, the difference between the maximum and average temperatures has been reduced after the threshold introduction. This difference for proposed design compared to conventional design has been decreased by 2.8 K, 1.6 K, 1.0 K and 1.9 K for rectangular, trapezoidal, triangular and concave manifold cases respectively.

The temperature distribution in heat exchangers is of great importance for the end-users. The uniformity of temperature profile ensures, for example, that the chemical process will proceed as intended (if it is temperature-dependent) or that the working fluid will change its phase throughout the entire exchanger and not just part of it.

The velocity distribution of fluid over the minigap section for various manifolds has been shown in Fig. 17 and Fig. 18 (conventional and threshold case respectively). The velocity profiles do not differ

qualitatively depends on a manifold. It can be seen that fluid flow diagonally through the minigap section in both cases (conventional and threshold case). Nevertheless, introducing the threshold provides more uniform flow. The areas where velocity is near 0 m/s near edges of minigap are getting smaller. Comparing Fig. 13 and Fig. 17 or Fig. 14 and Fig. 18 shows clearly that the minigap section suffers more from maldistribution phenomena.

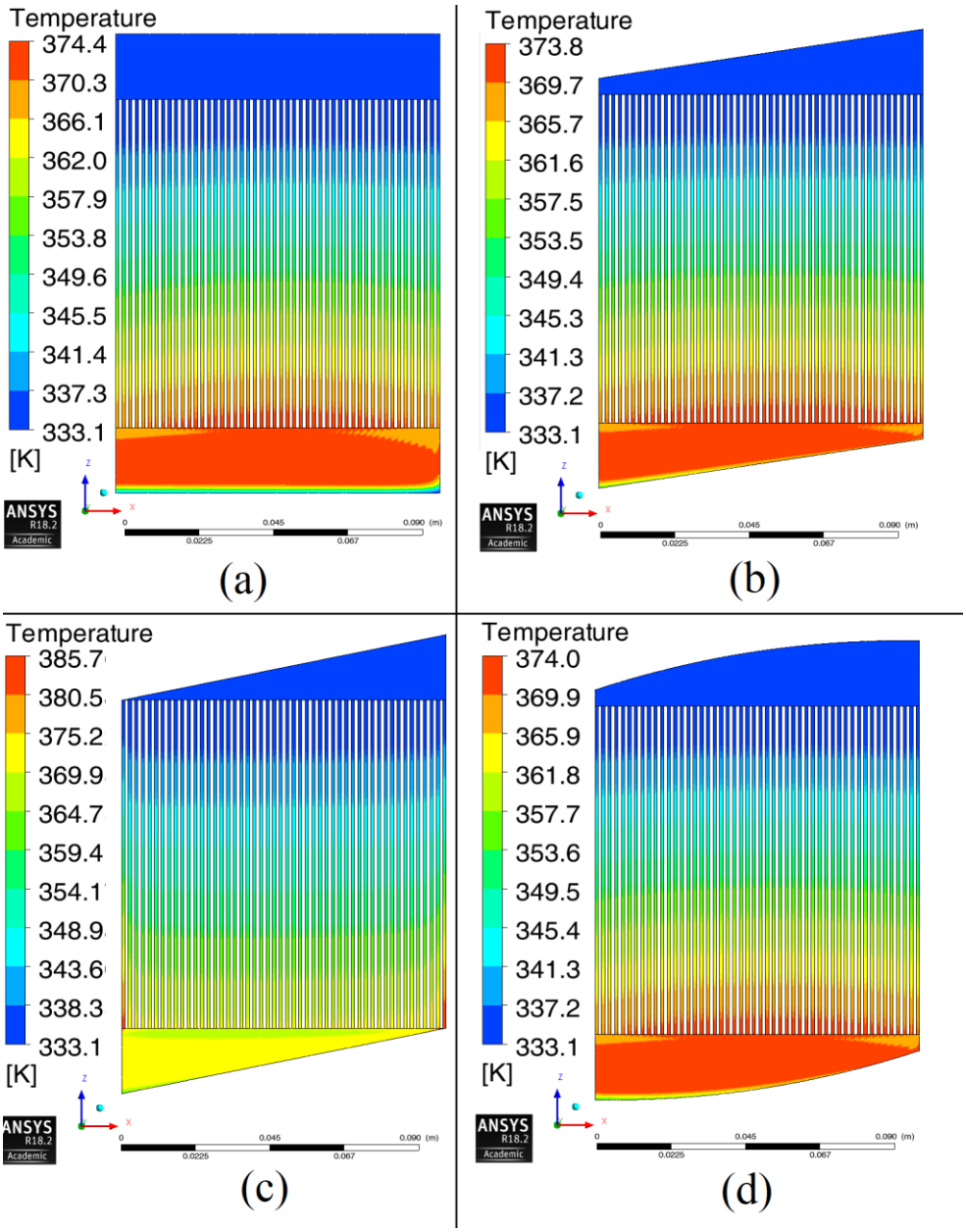

Fig. 16 The temperature distribution over minichannel heat exchanger with various manifolds (novel case with threshold). Manifolds: (a) rectangular (b) trapezoidal (c) triangular (d) concave.

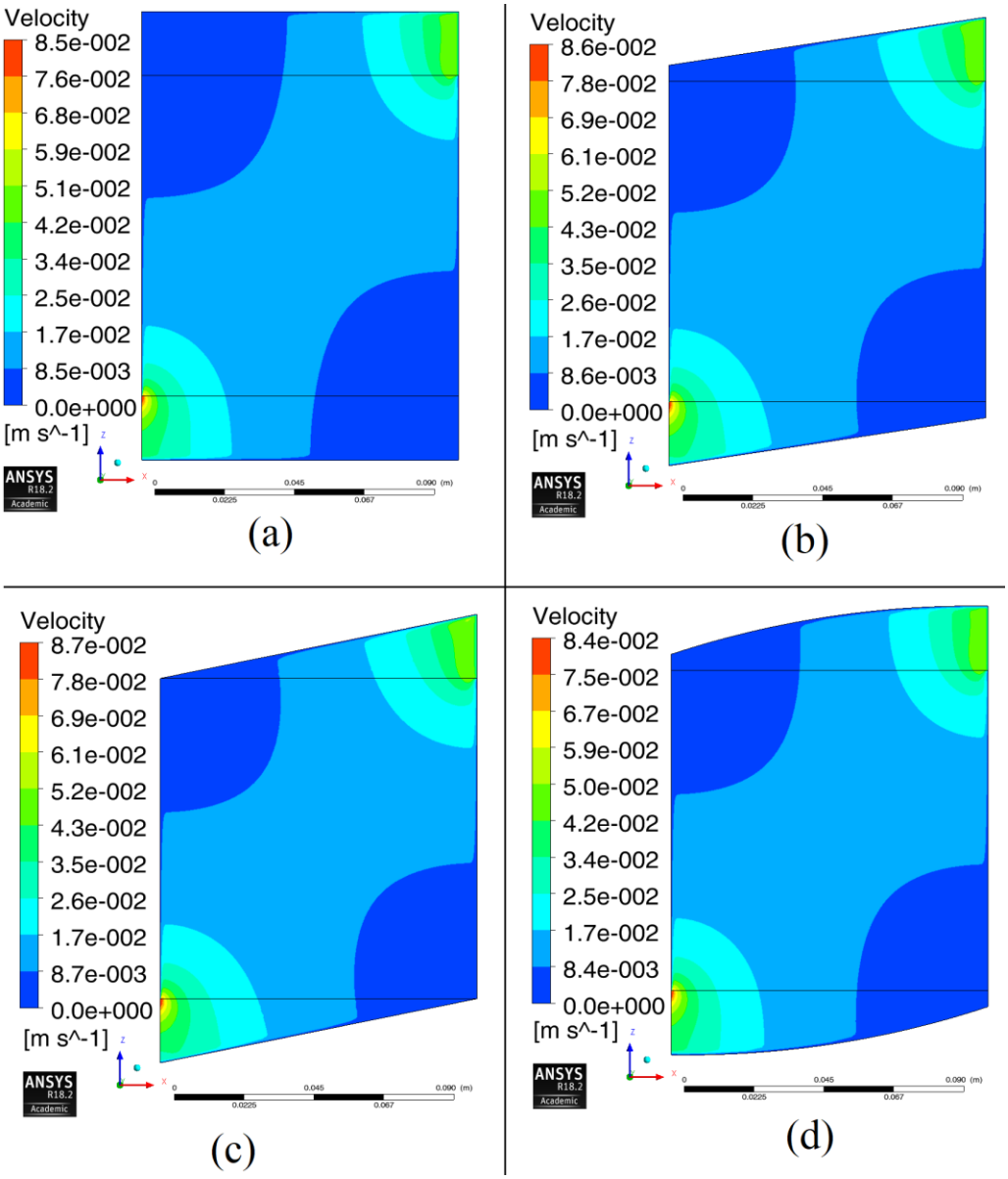

Fig. 17 The velocity distribution over minigap heat exchanger with various manifolds (conventional case without threshold). Manifolds: (a) rectangular (b) trapezoidal (c) triangular (d) concave.

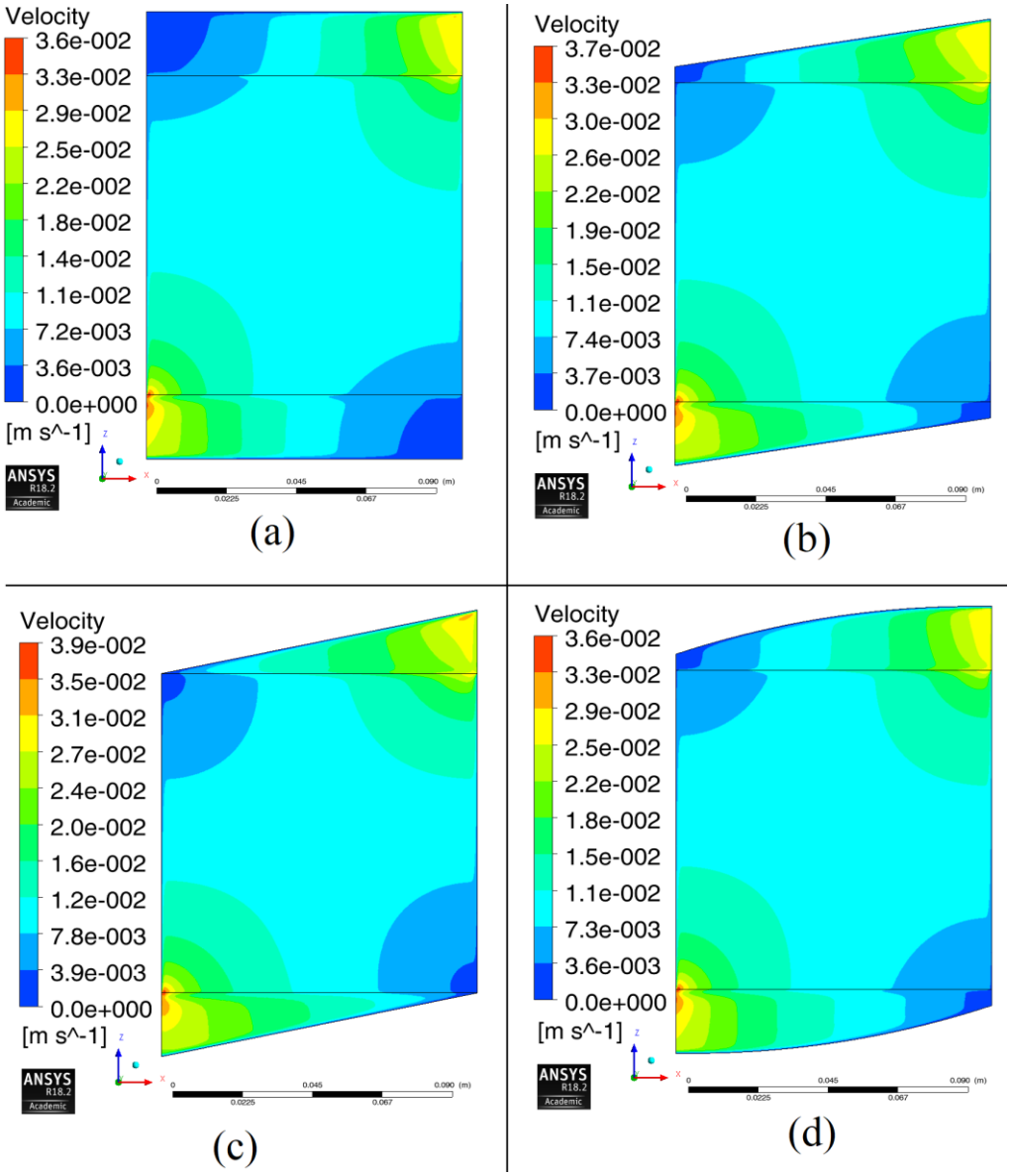

Fig. 18 The velocity distribution over minigap heat exchanger with various manifolds (novel case with threshold). Manifolds: (a) rectangular (b) trapezoidal (c) triangular (d) concave.

The profiles of the maldistribution coefficient over the XZ surface of the minigap for conventional and novel manifolds have been shown in Fig. 19, Fig. 20, Fig. 21 and Fig. 22. To make figures more clear, only ten points (out of fifty) in the X-axis direction have been shown. It can be seen that the maldistribution coefficient is not the same in all planes along the Z-axis. It is the highest in XY planes near the inlet and outlet and the lowest in the middle of the minigap (Z=50 mm). This phenomenon does not occur in minichannel sections, because the amount of fluid that has flowed into the channel is constant along with it. Due to the aforementioned diagonal flow in the minigap sections, maldistribution coefficients are the highest at the inlet and outlet of the minigap. Moreover, the minimum of maldistribution coefficient in every XY plane moves closer to the outlet (X=40 mm in the first XY plane and X=80 mm in the last XY plane).

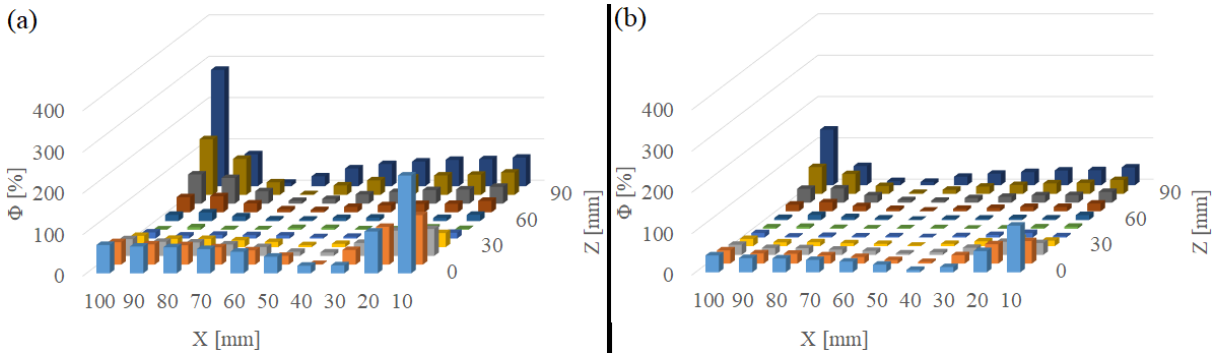

Fig. 19 The maldistribution coefficient profiles for minigap section with rectangular manifolds. (a) conventional case (without threshold) (b) novel case (with threshold).

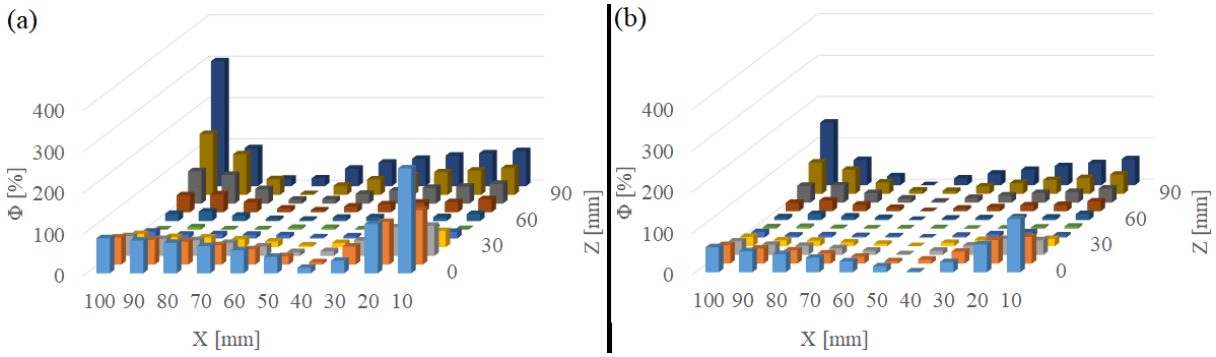

Fig. 20 The maldistribution coefficient profiles for minigap section with trapezoidal manifolds. (a) conventional case (without threshold) (b) novel case (with threshold).

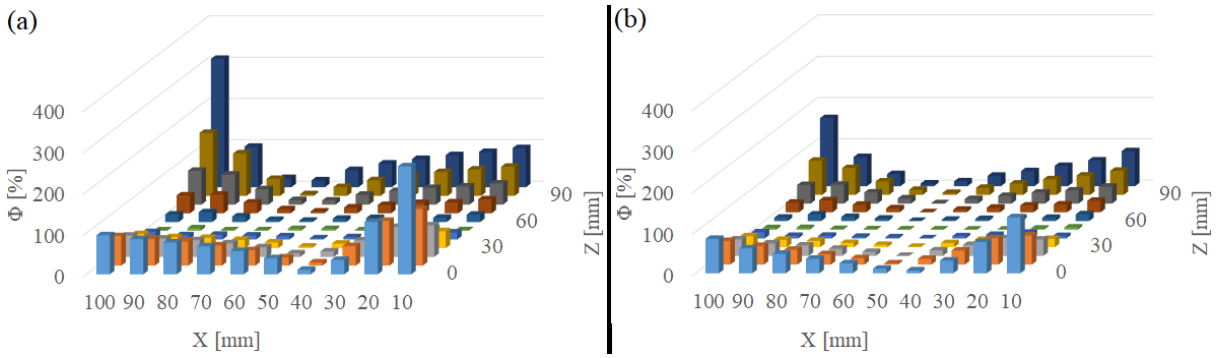

Fig. 21 The maldistribution coefficient profiles for minigap section with triangular manifolds. (a) conventional case (without threshold) (b) novel case (with threshold).

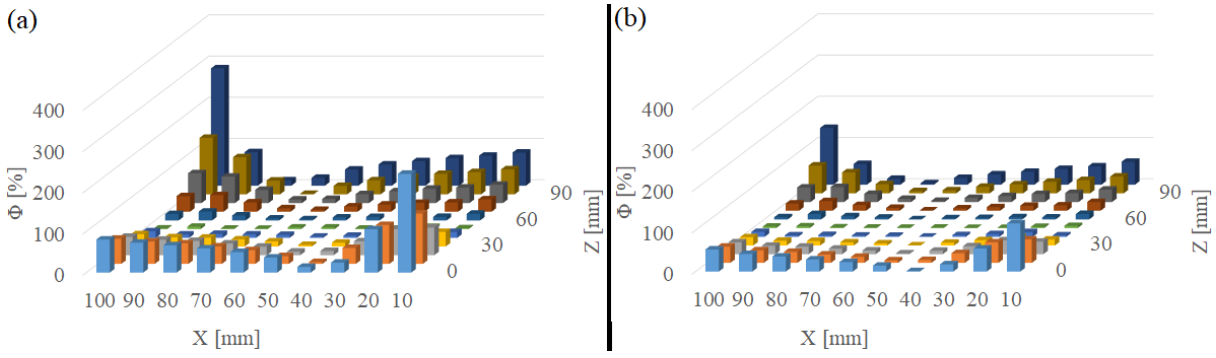

Fig. 22 The maldistribution coefficient profiles for minigap section with concave manifolds. (a) conventional case (without threshold) (b) novel case (with threshold).

The temperature profile in the minigap section is also more non-uniform than the temperature profile in the minichannel section. The temperatures over the minigap heat exchanger with various

conventional manifolds have been shown in Fig. 23. The hotspots have higher temperatures than those in minichannel sections. Introducing threshold at the entrance of the minigeometry section improves the temperature profile, as can be seen in Fig. 24. The maximum temperature reduction is 7 K, 6.4 K, 0.3 K and 8.1 K for rectangular, trapezoidal, triangular and concave manifold respectively. The difference between the maximum and average temperature for the proposed design compared to conventional design has been decreased by 6.5 K, 6.6 K, 0.2 K and 8.2 K for rectangular, trapezoidal, triangular and concave manifold cases respectively. As can be seen, these values are much better than those for the corresponding manifolds in a minichannel section. Nevertheless, the absolute values of the difference between the maximum and average temperatures for minigap sections are still higher than those for minichannel sections.

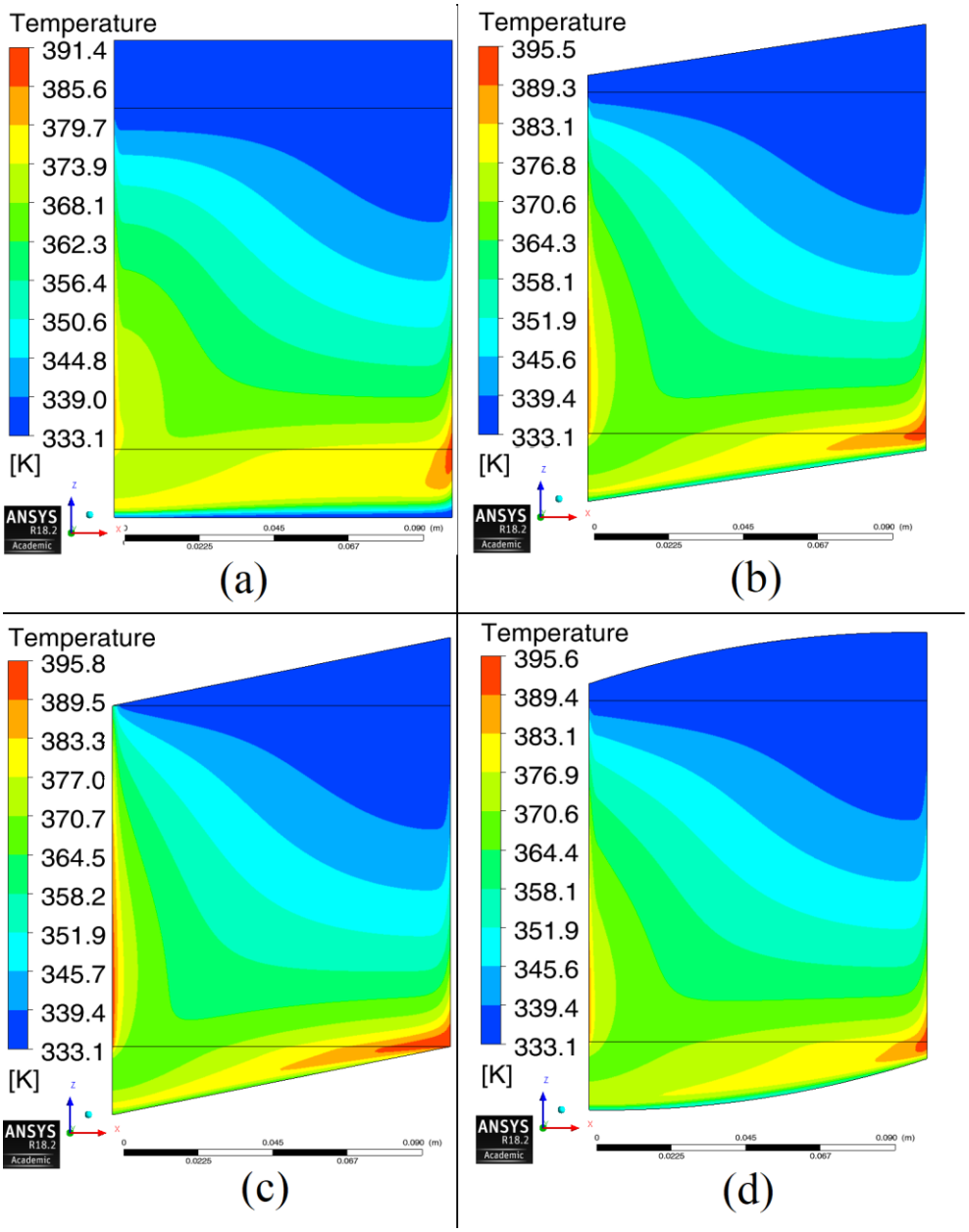

Fig. 23 The temperature distribution over minigap heat exchanger with various manifolds (conventional case without threshold). Manifolds: (a) rectangular (b) trapezoidal (c) triangular (d) concave.

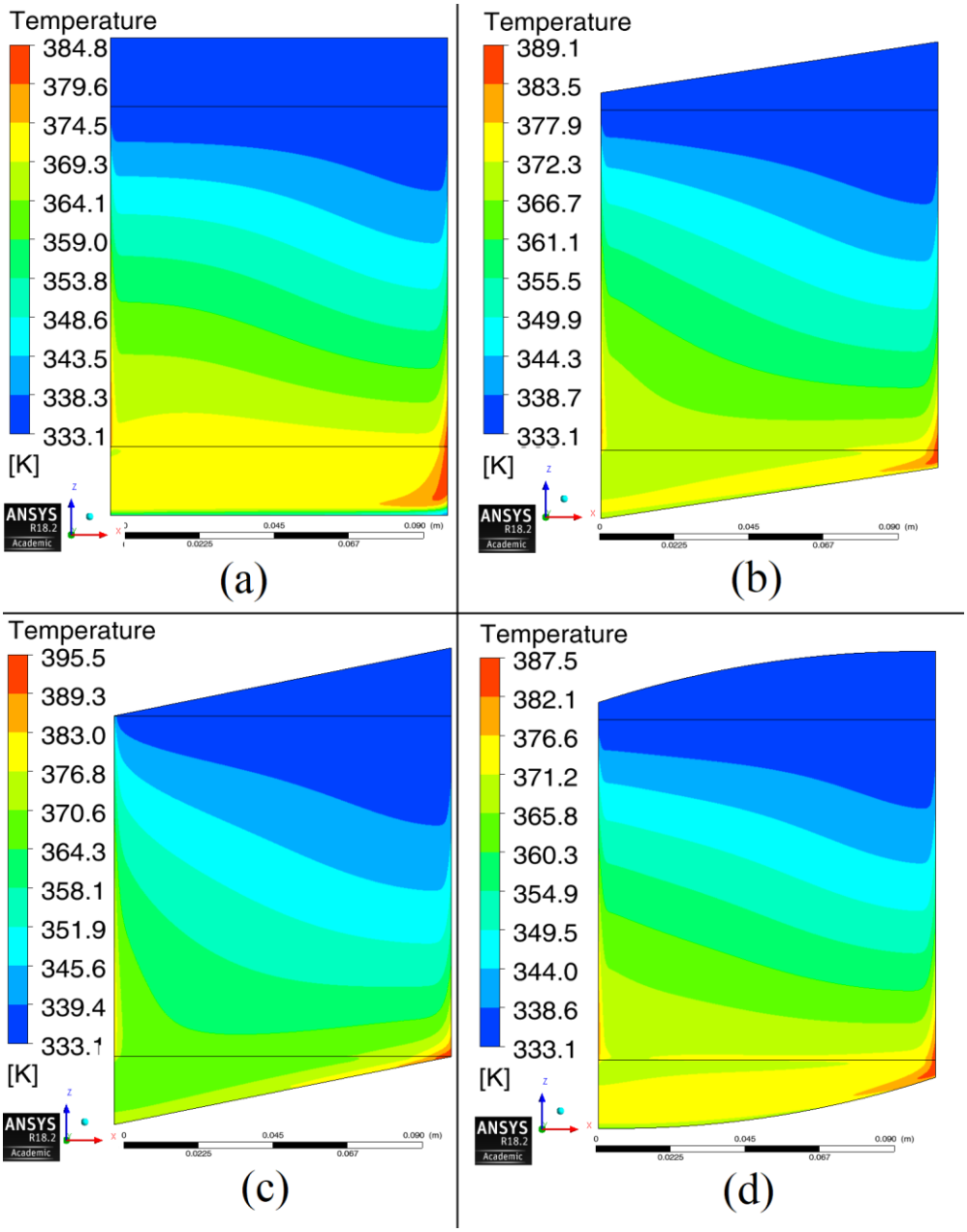

Fig. 24 The temperature distribution over minigap heat exchanger with various manifolds (novel case with threshold). Manifolds: (a) rectangular (b) trapezoidal (c) triangular (d) concave.

Another parameter that is of great importance for the working fluid distribution in the heat exchanger is the pressure drop. It is known that to obtain the uniform distribution of fluid in a whole heat exchanger, the pressure drop in every channel should be the same. It can be deduced from some works [42,43] that the parameter which influences the flow maldistribution is the ratio of pressure drop in channels to total pressure drop in a heat exchanger. When this pressure drop ratio is closer to 1, then flow becomes more uniform.

The pressure drop analysis in minichannel cases was presented in Table 3 and Table 4. First of all, the pressure drop in channels is not changing after the threshold introduction, which is understandable. Moreover, novel cases have an increased pressure drop ratio compared to conventional cases. It is so, due to the higher hydraulic diameter of manifolds and hence lower friction losses in them. The highest pressure drops in manifolds (and the lowest pressure drop ratios) are for triangular geometries and the lowest for rectangular geometries. This explains the highest flow maldistribution coefficients for

triangular geometry and the lowest for the rectangular one before the threshold introduction (Fig. 10). However, for the novel cases, the highest pressure drop ratio (rectangular geometry) does not correspond with the lowest flow maldistribution coefficient (trapezoidal and concave geometries) as can be deduced from Fig. 10 and Table 4.

It shows that introducing the threshold in manifolds makes the flow more uniform not only thanks to lowering the pressure drop in manifolds but also stabilize flow in them. The pressure drop ratio is not the only parameter that influences and describes the flow non-uniformity.

Table 3 Pressure drop in the inlet manifold, section and outlet manifold for minichannel section with various manifolds' geometry without threshold (conventional case)

	Inlet manifold [Pa]	**Section [Pa]**	**Outlet manifold [Pa]**	**Pressure drop ratio [-]**
Rectangular	15.7	41.5	16.2	0.57
Trapezoidal	20.5	41.5	20.8	0.50
Triangular	25.0	41.5	25.1	0.45
Concave	17.1	41.5	17.6	0.54

Table 4 Pressure drop in the inlet manifold, section and outlet manifold for minichannel section with various manifolds' geometry with the threshold (novel case)

	Inlet manifold [Pa]	**Section [Pa]**	**Outlet manifold [Pa]**	**Pressure drop ratio [-]**
Rectangular	5.0	41.5	5.1	0.80
Trapezoidal	6.6	41.5	6.6	0.76
Triangular	8.2	41.5	8.2	0.72
Concave	5.5	41.5	5.6	0.79

It can be seen also from Table 5 and Table 6 analysis. First of all, pressure drop ratios for minigap cases are lower than pressure drop ratios for minichannel cases before threshold introduction and after introducing it as well. That can partially explain higher flow maldistribution coefficients for minigap cases than minichannel cases. The novel cases are characterized by higher pressure drop ratios than the conventional ones. Worth to notice, that pressure drop ratios for minigap sections with the threshold (Table 6) are almost the same as for the minichannel sections without threshold (Table 3). Nevertheless, flow maldistribution coefficients are still much higher for minigap cases (118% ÷ 164%) than minichannel cases (23% ÷ 46%) as can be seen in Fig. 10 and Fig. 12. It is so, due to the two-dimensional character of flow in minigap, compared to one-dimensional in minichannels.

The pressure drop ratio cannot be the only parameter that testifies the uniformity of flow. It is true that an increase in this parameter results in a qualitative improvement in fluid distribution. However, identical pressure drop ratios cannot quantitatively indicate equal maldistribution coefficients.

Table 5 Pressure drop in the inlet manifold, section and outlet manifold for minigap section with various manifolds' geometry without threshold (conventional case)

	Inlet manifold [Pa]	**Section [Pa]**	**Outlet manifold [Pa]**	**Pressure drop ratio [-]**
Rectangular	9.2	9.1	9.7	0.32
Trapezoidal	10.2	9.1	10.5	0.31
Triangular	10.5	9.1	10.8	0.30
Concave	9.4	9.1	9.9	0.32

Table 6 Pressure drop in the inlet manifold, section and outlet manifold for minigap section with various manifolds' geometry with the threshold (novel case)

	Inlet manifold [Pa]	Section [Pa]	Outlet manifold [Pa]	Pressure drop ratio [-]
Rectangular	3.7	9.1	3.9	0.54
Trapezoidal	4.3	9.1	4.5	0.51
Triangular	4.7	9.1	4.9	0.48
Concave	3.8	9.1	4.1	0.53

5. Conclusions

A detailed numerical investigation was performed to investigate the effect of threshold introduction on the thermohydraulic maldistribution in mini heat exchangers. A minichannel and minigap sections fed by conventional manifolds without a threshold and with 0.5 mm threshold at the entrance to the section have been considered. The presented approach is new in terms of flows with heat exchange and the two-dimensional maldistribution calculations in the minigap section have not been found in literature yet. Based on the above results, the following conclusions were made.

The 0.5 mm high threshold before the minigeometry section provides the possibility to stabilize flow and distribute fluid to every channel or over the width of the gap equally. The maldistribution coefficient can be reduced about three times in the minichannel section and about two times in the minigap section.

Regardless of the manifold's shape, more uniform distribution can be observed in the minichannel section than in the minigap section. The minigap section suffers more from non-uniform distribution of fluid due to two-dimensional flow over a minigap in comparison to one-dimensional flow in channels.

The reduction of flow maldistribution results in a more uniform temperature profile over the heat exchanger's surface. Moreover, the highest temperature is reduced even by 8 K by introducing a small threshold at the entrance of the mini section.

Due to the high maldistribution for a minigap section, the isotherms lines are distorted and significantly diverge from lines perpendicular to the direction of the flow that would occur for perfectly even distribution. The described flow maldistribution reduction approach improves the uniformity and makes the isotherms lines less distorted.

The proposed approach of maldistribution mitigation is easy to implement. This requires only a few additional operations during the machining of the heat exchanger. It reduces the overall pressure drop in heat exchanger while maintaining the heat transfer coefficients at a similar level. However, the most important is the reduction of maximum temperature and the difference between the maximum and the average temperature in a heat exchanger for minichannel and minigap sections.

6. Acknowledgments

The work presented in this paper was funded from the National Science Centre, Poland research project No. 2017/27/N/ST8/02785 in the years 2018-2020.

7. Nomenclature

C_p – Specific heat of fluid, J/kg K
D – Depth, mm
D_h – Hydraulic diameter, mm
k_f – Fluid thermal conductivity, W/m K
N – Number of points
Nu – Nusselt number
L – Channel length, m
p – Pressure, Pa
q – Heat flux, W/m^2

T – Temperature, K
t – Threshold's height, mm
V – Velocity, m/s

Greek symbols
μ – Dynamic viscosity, Pa s
ρ – Density, kg/m^3
Φ – Maldistribution coefficient

Subscripts
avg – Average
f – Fluid
i – i-th channel/point
m – Mean
n – Normalized
o – Overall
w – Wall

Abbreviations
FVM – Finite volume method
SST – Shear stress transport

8. References

[1] D.B. Tuckerman, R.F.W. Pease, High-performance heat sinking for VLSI, IEEE Electron Device Lett. 2 (1981) 126–129. doi:10.1109/EDL.1981.25367.

[2] M. Bahreini, A. Ramiar, A.A. Ranjbar, Numerical simulation of subcooled flow boiling under conjugate heat transfer and microgravity condition in a vertical mini channel, Appl. Therm. Eng. 113 (2017) 170–185. doi:10.1016/j.applthermaleng.2016.11.016.

[3] J. Zhou, X. Zhao, X. Ma, Z. Du, Y. Fan, Y. Cheng, X. Zhang, Clear-days operational performance of a hybrid experimental space heating system employing the novel mini-channel solar thermal & PV/T panels and a heat pump, Sol. Energy. 155 (2017) 464–477. doi:10.1016/j.solener.2017.06.056.

[4] D. Mikielewicz, J. Mikielewicz, A thermodynamic criterion for selection of working fluid for subcritical and supercritical domestic micro CHP, Appl. Therm. Eng. 30 (2010) 2357–2362. doi:10.1016/j.applthermaleng.2010.05.035.

[5] K. Sakamatapan, S. Wongwises, Pressure drop during condensation of R134a flowing inside a multiport minichannel, Int. J. Heat Mass Transf. 75 (2014) 31–39. doi:https://doi.org/10.1016/j.ijheatmasstransfer.2014.02.071.

[6] M. Najim, M.B. Feddaoui, New cooling approach using successive evaporation and condensation of a liquid film inside a vertical mini-channel, Int. J. Heat Mass Transf. 122 (2018) 895–912. doi:10.1016/j.ijheatmasstransfer.2018.02.034.

[7] M. Khoshvaght-Aliabadi, M. Sahamiyan, M. Hesampour, O. Sartipzadeh, Experimental study on cooling performance of sinusoidal-wavy minichannel heat sink, Appl. Therm. Eng. 92 (2016) 50–61. doi:10.1016/j.applthermaleng.2015.09.015.

[8] C. Qi, X. Chen, W. Wang, J. Miao, H. Zhang, Experimental investigation on flow condensation heat transfer and pressure drop of nitrogen in horizontal tubes, Int. J. Heat Mass Transf. 132 (2019) 985–996. doi:10.1016/j.ijheatmasstransfer.2018.11.092.

[9] J.R. García-Cascales, F. Illán-Gómez, F. Hidalgo-Mompeán, F.A. Ramírez-Rivera, M.A. Ramírez-Basalo, Performance comparison of an air/water heat pump using a minichannel coil as evaporator in replacement of a fin-and-tube heat exchanger, Int. J. Refrig. 74 (2017) 558–573. doi:10.1016/j.ijrefrig.2016.11.018.

[10] C. Pistoresi, Y. Fan, L. Luo, Numerical study on the improvement of flow distribution uniformity among parallel mini-channels, Chem. Eng. Process. Process Intensif. 95 (2015) 63–71. doi:https://doi.org/10.1016/j.cep.2015.05.014.
[11] C. Amador, A. Gavriilidis, P. Angeli, Flow distribution in different microreactor scale-out geometries and the effect of manufacturing tolerances and channel blockage, Chem. Eng. J. 101 (2004) 379–390. doi:10.1016/j.cej.2003.11.031.
[12] H. Yang, J. Wen, X. Gu, Y. Liu, S. Wang, W. Cai, Y. Li, A mathematical model for flow maldistribution study in a parallel plate-fin heat exchanger, Appl. Therm. Eng. 121 (2017) 462–472. doi:10.1016/j.applthermaleng.2017.03.130.
[13] S. Kakaç, H. Liu, A. Pramuanjaroenkij, Heat Exchangers, Boca Raton: CRC Press, 2002. doi:10.1201/9781420053746.
[14] P. Dąbrowski, M. Klugmann, D. Mikielewicz, Channel Blockage and Flow Maldistribution during Unsteady Flow in a Model Microchannel Plate heat Exchanger, J. Appl. Fluid Mech. 12 (2019) 1023–1035. doi:10.29252/jafm.12.04.29316.
[15] A.A.Y. Al-Waaly, M.C. Paul, P. Dobson, Liquid cooling of non-uniform heat flux of a chip circuit by subchannels, Appl. Therm. Eng. 115 (2017) 558–574. doi:10.1016/j.applthermaleng.2016.12.061.
[16] V. Manoj Siva, A. Pattamatta, S.K. Das, Effect of flow maldistribution on the thermal performance of parallel microchannel cooling systems, Int. J. Heat Mass Transf. 73 (2014) 424–428. doi:10.1016/j.ijheatmasstransfer.2014.02.017.
[17] J. Kim, J.H. Shin, S. Sohn, S.H. Yoon, Analysis of non-uniform flow distribution in parallel micro-channels, J. Mech. Sci. Technol. 33 (2019) 3859–3864. doi:10.1007/s12206-019-0729-8.
[18] H. Li, P. Hrnjak, Quantification of liquid refrigerant distribution in parallel flow microchannel heat exchanger using infrared thermography, Appl. Therm. Eng. 78 (2015) 410–418. doi:10.1016/j.applthermaleng.2015.01.003.
[19] V. Singh, H. Kumar, S.S. Sehgal, R. Kukreja, Effect of Plenum Shape on Thermohydraulic Performance of Microchannel Heat Sink, J. Inst. Eng. Ser. C. (2019). doi:10.1007/s40032-019-00515-z.
[20] M. Klugmann, P. Dabrowski, D. Mikielewicz, Pressure drop related to flow maldistribution in a model minichannel plate heat exchanger, Arch. Thermodyn. 39 (2018) 123–146. doi:10.1515/aoter-2018-0015.
[21] W. Zhou, W. Deng, L. Lu, J. Zhang, L. Qin, S. Ma, Y. Tang, Laser micro-milling of microchannel on copper sheet as catalyst support used in microreactor for hydrogen production, Int. J. Hydrogen Energy. 39 (2014) 4884–4894. doi:10.1016/j.ijhydene.2014.01.041.
[22] S. Kumar, P.K. Singh, Effects of flow inlet angle on flow maldistribution and thermal performance of water cooled mini-channel heat sink, Int. J. Therm. Sci. 138 (2019) 504–511. doi:10.1016/j.ijthermalsci.2019.01.014.
[23] P. Dąbrowski, M. Klugmann, D. Mikielewicz, Selected studies of flow maldistribution in a minichannel plate heat exchanger, Arch. Thermodyn. 38 (2017) 135–148. doi:10.1515/aoter-2017-0020.
[24] J. Mathew, P.S. Lee, T. Wu, C.R. Yap, Experimental study of flow boiling in a hybrid microchannel-microgap heat sink, Int. J. Heat Mass Transf. 135 (2019) 1167–1191. doi:10.1016/j.ijheatmasstransfer.2019.02.033.
[25] A. Tamanna, P.S. Lee, Flow boiling heat transfer and pressure drop characteristics in expanding silicon microgap heat sink, Int. J. Heat Mass Transf. 82 (2015) 1–15. doi:10.1016/j.ijheatmasstransfer.2014.11.047.
[26] T. Alam, P.S. Lee, C.R. Yap, L. Jin, A comparative study of flow boiling heat transfer and pressure drop characteristics in microgap and microchannel heat sink and an evaluation of microgap heat sink for hotspot mitigation, Int. J. Heat Mass Transf. 58 (2013) 335–347. doi:10.1016/j.ijheatmasstransfer.2012.11.020.
[27] L.S. Maganti, P. Dhar, T. Sundararajan, S.K. Das, Heat spreader with parallel microchannel configurations employing nanofluids for near–active cooling of MEMS, Int. J. Heat Mass

Transf. 111 (2017) 570–581. doi:10.1016/j.ijheatmasstransfer.2017.04.032.
[28] A. Gorodetsky, T. Rozenfeld, H.D. Haustein, G. Ziskind, Flow and heat transfer analysis of hybrid cooling schemes: Adding micro-jets to a micro-gap, Int. J. Therm. Sci. 138 (2019) 367–383. doi:10.1016/j.ijthermalsci.2019.01.015.
[29] M. Piasecka, K. Strąk, B. Maciejewska, Calculations of Flow Boiling Heat Transfer in a Minichannel Based on Liquid Crystal and Infrared Thermography Data, Heat Transf. Eng. 38 (2017) 332–346. doi:10.1080/01457632.2016.1189272.
[30] K. Strąk, M. Piasecka, B. Maciejewska, Spatial orientation as a factor in flow boiling heat transfer of cooling liquids in enhanced surface minichannels, Int. J. Heat Mass Transf. 117 (2018) 375–387. doi:10.1016/j.ijheatmasstransfer.2017.10.019.
[31] M. Saeed, M.H. Kim, Header design approaches for mini-channel heatsinks using analytical and numerical methods, Appl. Therm. Eng. 110 (2017) 1500–1510. doi:10.1016/j.applthermaleng.2016.09.069.
[32] W. Tang, L. Sun, H. Liu, G. Xie, Z. Mo, J. Tang, Improvement of flow distribution and heat transfer performance of a self-similarity heat sink with a modification to its structure, Appl. Therm. Eng. 121 (2017) 163–171. doi:10.1016/j.applthermaleng.2017.04.051.
[33] R. Kumar, G. Singh, D. Mikielewicz, A New Approach for the Mitigating of Flow Maldistribution in Parallel Microchannel Heat Sink, J. Heat Transfer. 140 (2018) 72401–72410. http://dx.doi.org/10.1115/1.4038830.
[34] R. Kumar, G. Singh, D. Mikielewicz, Numerical Study on Mitigation of Flow Maldistribution in Parallel Microchannel Heat Sink: Channels Variable Width Versus Variable Height Approach, J. Electron. Packag. 141 (2019) 21009–21011. http://dx.doi.org/10.1115/1.4043158.
[35] C. Anbumeenakshi, M.R. Thansekhar, Experimental investigation of header shape and inlet configuration on flow maldistribution in microchannel, Exp. Therm. Fluid Sci. 75 (2016) 156–161. doi:10.1016/j.expthermflusci.2016.02.004.
[36] P. Dąbrowski, Mitigation of Flow Maldistribution in Minichannel and Minigap Heat Exchangers by Introducing Threshold in Manifolds, J. Appl. Fluid Mech. 13 (2020) 815–826. doi:10.29252/jafm.13.03.30454.
[37] K. Dhinsa, C. Bailey, K. Pericleous, Investigation into the performance of turbulence models for fluid flow and heat transfer phenomena in electronic applications, IEEE Trans. Components Packag. Technol. 28 (2005) 686–699. doi:10.1109/TCAPT.2005.859758.
[38] C.S. Sharma, M.K. Tiwari, B. Michel, D. Poulikakos, Thermofluidics and energetics of a manifold microchannel heat sink for electronics with recovered hot water as working fluid, Int. J. Heat Mass Transf. 58 (2013) 135–151. doi:10.1016/j.ijheatmasstransfer.2012.11.012.
[39] P.S. Lee, S. V. Garimella, Thermally developing flow and heat transfer in rectangular microchannels of different aspect ratios, Int. J. Heat Mass Transf. 49 (2006) 3060–3067. doi:10.1016/j.ijheatmasstransfer.2006.02.011.
[40] J.M. Commenge, L. Falk, J.P. Corriou, M. Matlosz, Optimal Design for Flow Uniformity in Microchannel Reactors, AIChE J. 48 (2002) 345–358. doi:10.1002/aic.690480218.
[41] P. Minqiang, Z. Dehuai, T. Yong, C. Dongqing, CFD-based study of velocity distribution among multiple parallel microchannels, J. Comput. 4 (2009) 1133–1138. doi:10.4304/jcp.4.11.1133-1138.
[42] I.A. Ghani, N.A. Che Sidik, N. Kamaruzzaman, W. Jazair Yahya, O. Mahian, The effect of manifold zone parameters on hydrothermal performance of micro-channel HeatSink: A review, Int. J. Heat Mass Transf. 109 (2017) 1143–1161. doi:10.1016/j.ijheatmasstransfer.2017.03.007.
[43] S.S. Sehgal, K. Murugesan, S.K. Mohapatra, Effect of channel and plenum aspect ratios on the performance of microchannel heat sink under different flow arrangements, J. Mech. Sci. Technol. 26 (2012) 2985–2994. doi:10.1007/s12206-012-0705-z.